^{81}Br and ^{35}Cl NMR Investigation of Sodium,Silver,Halo-Sodalite Semiconductor Supralattices

Raz Jelinek,[†] Andreas Stein,[‡,§] and Geoffrey A. Ozin*[,§]

Contribution from the Materials Sciences Division, Lawrence Berkeley Laboratory, and Department of Chemistry, University of California, Berkeley, California 94720, and Advanced Zeolite Materials Science Research Group, Lash Miller Chemical Laboratories, University of Toronto, 80 St. George Street, Toronto, Ontario, Canada M5S 1A1. *Received May 14, 1992*

Abstract: ^{81}Br and ^{35}Cl NMR yields, respectively, bromide and chloride site-specific information pertinent to the structural and electronic properties of $Na_{8-n-p}Ag_nX_{2-p}$-sodalite, semiconductor cluster supralattices, where X = Br, Cl; $0 \le n \le 8$; $0 \le p \le 2$. The ^{81}Br and ^{35}Cl MAS chemical shifts and line shapes observed for encapsulated Na_4X and Ag_4X clusters within the sodalite cavities provide insight into the nature of the intracluster bonding (ionic-covalent character) and the extent of intercavity coupling. Substantial nuclear shielding is observed for encapsulated Ag_4X clusters in sodalite materials with high loading of Ag_4Br clusters, whereas no NMR signal is detected from silver-bromide clusters isolated within sodalite lattices. Spin-lattice and spin-spin relaxation measurements yield information on intracavity coupling and motion within the sodalite cages. The results enable one to explore the transition from isolated clusters to an expanded Ag_4X supralattice, through the compositional and temperature dependence of the NMR spectra of the sodalite halide anions.

Introduction

The cuboctahedral pore structure of sodalites enables them to host insulator, semiconductor, or metal cluster guests of uniform size and shape.[1] This unique quality may provide potential uses for these nanoporous solids as expanded metal or even superconducting arrays[2] and semiconductor cluster supralattices which are of interest in quantum electronics, nonlinear optics, and information storage and processing.[1,3] A recent example concerns the sodalite materials denoted $Na_{8-n-p}Ag_nX_{2-p}$-sodalite ($0 \le n \le 8$; $0 \le p \le 2$; X = Br, Cl; and sodalite = $Si_6Al_6O_{12}$). Through silver ion exchange of sodium,halo-sodalites, the encapsulated sodium,silver-halide guests can be transformed from the isolated AgBr molecule to isolated $Na_{4-x}Ag_xBr$ clusters, and eventually to a supralattice of $Na_{4-x}Ag_xBr$ clusters ($0 \le x \le 4$).[4,5] These materials have been extensively investigated in our laboratories using several techniques, such as X-ray diffraction, infrared (IR) and optical spectroscopy,[5,6] and high-resolution solid-state NMR.[7]

Solid-state NMR investigations of porous aluminosilicates such as sodalites and zeolites have concentrated primarily on probing structural aspects of the framework nuclei ^{29}Si[8] and ^{27}Al.[9] To a lesser extent, extraframework charge-balancing cations such as ^{23}Na[10] have been studied, since these nuclei often give rise to quadrupolarly broadened spectral lines. In this context, anionic nuclei such as ^{35}Cl, ^{37}Cl, ^{79}Br, and ^{81}Br exhibit rather large quadrupolar interactions which limit their possible applications in solid-state NMR experiments. Some studies have used ^{35}Cl[11] and ^{79}Br[12] magic angle spinning (MAS) NMR to investigate inorganic halide salts which exhibit cubic symmetry.

In this work we describe ^{81}Br and ^{35}Cl NMR experiments, performed on Cl^- and Br^- anions distributed within the cavities of $Na_{8-n-p}Ag_nX_{2-p}$-sodalite lattices. High-resolution MAS spectra are produced which feature a profound sensitivity of the Cl^- and Br^- anions to the environments of the encapsulated Na_4X clusters. Significantly different chemical environments are observed for encapsulated Na_4X as compared to Ag_4X clusters, as well as for Ag_4X clusters in low and high abundance, within the sodalite lattice. ^{81}Br spin-lattice and spin-spin relaxation measurements indicate a difference between the dynamic properties of Br^- anions in the Na_4Br encapsulated clusters and the cation-exchanged Ag_4Br ones.

Experimental Section

The various sodium,silver,halo-sodalite samples were synthesized and analyzed by procedures described elsewhere.[6,13] NMR experiments were carried out in an 11.7-T magnetic field, on a Chemagnetics CMX-500 spectrometer fitted with a VT-MAS probe. The spinning speed in the MAS experiments was 5-6 kHz. In the one-pulse experiments we used short, 30°, radio-frequency (rf) pulses, with 300-ms delays.

Spin-lattice relaxation measurements (T_1) were carried out using the inversion-recovery pulse sequence (180°-τ-90°-acquisition), with recycle delays of more than $5T_1$ between each accumulation, in order to minimize saturation effects. Spin-spin relaxation experiments (T_2) were performed using a spin-echo pulse sequence (90°-τ-180°-acquisition). Low-power rf pulses were used in the relaxation experiments in order to guarantee a selective excitation of the central transition. Independent verification of selective excitation at room temperature was achieved by comparing the signal intensities at different pulse lengths (a nutation experiment[14]). From 5000 to 10000 acquisitions were accumulated, and 250-Hz Lorentzian apodization was applied to the spectra. The external references used were 0.1 M NaCl and 0.1 M NaBr for the ^{35}Cl and ^{81}Br experiments, respectively.

Results and Discussion

^{81}Br MAS Studies. Figure 1 shows ^{81}Br MAS spectra obtained for Br^- anions encapsulated within the supercages of sodium zeolite Y, Figure 1 (top), and the β-cages within the sodalite lattice, Figure 1 (bottom). The $^{81}Br^-$ anions interacting with the Na^+ cations in the spacious supercages of zeolite Y experience a highly asymmetrical charge distribution,[15] thus giving rise to the ex-

* To whom correspondence should be addressed.
† University of California.
‡ Current address: Department of Chemistry, University of Texas, Austin, TX 78712.
§ University of Toronto.

(1) Ozin, G. A.; Kuperman, A.; Stein, A. *Angew. Chem.* **1989**, *101*, 359. Ozin, G. A. *Adv. Mater. (Weinheim, Fed. Repub. Ger.)* **1992**, *4*, 612.
(2) Zhu, Y.; Huang, D.; Feng, S. *Phys. Rev. B* **1989**, *40*, 3169.
(3) Ozin, G. A.; Kirkby, S.; Meszaros, M.; Özkar, S.; Stein, A.; Stucky, G. D. In *Materials for Nonlinear Optics*; Marder, S. R., Sohn, J. E., Stucky, G. D., Eds.; ACS Symposium Series 455; American Chemical Society: Washington, DC, 1991; pp 554-581.
(4) Stein, A.; Ozin, G. A.; Stucky, G. D. *J. Am. Chem. Soc.* **1990**, *112*, 904.
(5) Stein, A.; Macdonald, P. M.; Ozin, G. A.; Stucky, G. M. *J. Phys. Chem.* **1990**, *94*, 6943.
(6) Stein, A.; Ozin, G. A.; Macdonald, G. M.; Stucky, G. D.; Jelinek, R. *J. Am. Chem. Soc.* **1992**, *114*, 5171.
(7) Jelinek, R.; Chmelka, B. F.; Stein, A.; Ozin, G. A. *J. Phys. Chem.* **1992**, *96*, 6744.
(8) Fyfe, C. A.; Thomas, J. M.; Klinowski, J.; Gobbi, G. C. *Angew. Chem.* **1983**, *22*, 259.
(9) Lippmaa, E.; Samoson, A.; Mägi, M. *J. Am. Chem. Soc.* **1986**, *108*, 1730.
(10) Tijink, G. A. H.; Janssen, R.; Veeman, W. S. *J. Am. Chem. Soc.* **1987**, *109*, 7301.
(11) Weeding, T. L.; Veeman, W. S. *J. Chem. Soc., Chem. Commun.* **1989**, 946.
(12) Zumbulyadis, N.; Marchetti, A. *Colloids Surf.* **1990**, *45*, 335.
(13) Stein, A. Ph.D. Thesis, University of Toronto, November 1991. Stein, A.; Ozin, G. A.; Stucky, G. D. *J. Am. Chem. Soc.* **1992**, *114*, 8119.
(14) Fenzke, D.; Freude, D.; Fröhlich, T.; Haase, J. *Chem. Phys. Lett.* **1984**, *111*, 171.

0002-7863/93/1515-2390$04.00/0

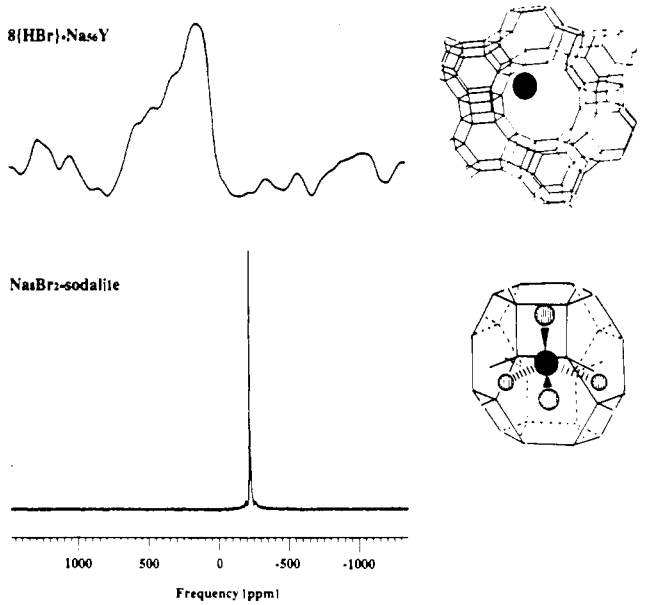

Figure 1. ^{81}Br MAS spectra and schematic drawings of Br^- encapsulated within the supercage of sodium zeolite Y in n{HBr}–$Na_{56}Y$ (top) and Br^- encapsulated within a sodalite cage in Na_8Br_2–sodalite (bottom).

tremely broad, ≈100-kHz, ^{81}Br MAS signal, Figure 1, top. A distribution of the Br^- anions within the available Na^+ cation sites within the supercage might further broaden the NMR line. The situation in the sodium,bromo–sodalite system is significantly different. The bromide anions are located at the center of the sodalite cages, tetrahedrally surrounded by four monovalent cations; see the schematic drawing in Figure 1, bottom. This arrangement provides a rather symmetrical environment for the ^{81}Br nuclei, thus reducing considerably the quadrupolar broadening of the spectral line, Figure 1, bottom. At room temperature there is no diffusion of either the Na^+ cations or the bromide anions between adjacent cages.[7]

Figure 2 shows the ^{81}Br MAS spectra of sodium,bromo–sodalites with different quantities of intentionally introduced halide-empty cages. The anion-free cavities are prepared in the initial synthesis stages[6,13] and contain three Na^+ cations as well as one to four water molecules. Each cavity within the sodalite matrix is surrounded by eight adjacent cages, in a body-centered cubic arrangement. Therefore, in each of the materials shown in Figure 2 there will be a different nearest-neighbor distribution of bromide-containing and bromide-empty cages. Examining the ^{81}Br signals from the encapsulated Na_4Br clusters in Figure 2 reveals a clear sensitivity of the Br^- anion to its surrounding cavities.

An upfield shoulder is observed in the ^{81}Br MAS spectrum of the sodalite material which exhibits a 2:1 ratio between the Br^--containing and Br^--free cages, respectively, Figure 2a. The shape of the ^{81}Br signal is not due to quadrupolar broadening, since double-rotation [DOR] experiments, which remove second-order quadruplar broadening, essentially produced identical spectra.[16] Therefore, the upfield shoulder arises probably from a distribution of Br^- environments, which is related to the occupancies of Br^--free cages adjacent to the Na_4Br clusters. Indeed, as the ratio of Br^--containing to Br^--free cages in the sample is reduced to 1:4, Figure 2b, and 1:9, Figure 2c, a broad component within the upfield shoulder increases substantially in intensity, and becomes the dominant signal in the latter compound. It has been demonstrated previously that the unit-cell size of the $Na_{8-p}Br_{2-p}$–sodalite enlarges with the complement of anion-free cages in the lattice.[5] The ionicity of the Na_4Br clusters increases in unison, localizing more negative charge on the bromide anion, causing it to experience a more shielded environment, as observed in Figure 2.

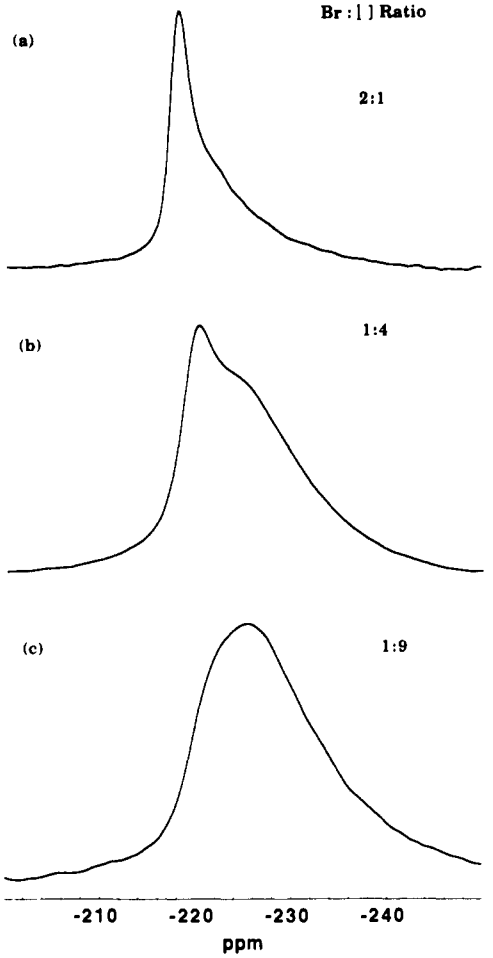

Figure 2. ^{81}Br MAS spectra of sodium,bromo–sodalite with different quantities of bromide-empty cavities: (a) $Na_{7.3}Br_{1.3}[\,]_{0.7}$–sodalite, (b) $Na_{6.4}Br_{0.4}[\,]_{1.6}$–sodalite, and (c) $Na_{6.2}Br_{0.2}[\,]_{1.8}$–sodalite ([ ] = bromide-empty cavities).

Room-temperature ^{81}Br spin–lattice relaxation measurements of a sodium,bromo–sodalite sample which contains ≈15% Br^--free cages, shown in Figure 3, support our interpretation of the data presented in Figure 2. Figure 3 features ^{81}Br MAS spectra, taken after various delay times τ, in the inversion–recovery pulse sequence. Two ^{81}Br sites, which exhibit significantly different spin–lattice relaxation rates, are clearly observed. The upfield shoulder exhibits a very fast spin–lattice relaxation rate and corresponds to ^{81}Br nuclei in cages which are adjacent to the anion-free cavities. The mobile water molecules contained in the bromide-free cavities introduce fluctuations of the electric-field gradients, which would substantially increase the spin–lattice relaxation of the neighboring ^{81}Br nuclei.[17]

Figure 4 features a series of silver-exchanged sodium,bromo–sodalites, $Na_{8-n}Ag_nBr_2$–sodalite, where $0 \le n \le 8$. The parent material, Na_8Br_2–sodalite, features a single peak at −219 ppm as shown in Figure 4b. This sample contains Na_4Br tetrahedra in approximately 90% of the cavities. The ^{81}Br peak which is ascribed to the Na_4Br clusters, Figure 4b, appears farther upfield, at −219 ppm, than the ^{81}Br MAS signal from bulk NaBr, at −7 ppm, Figure 4a. This shielding indicates a higher charge density around the Br^- anion for the Na_4Br tetrahedra in Na_8Br_2–sodalite, compared to the bulk NaBr.

As Ag^+ cations start replacing Na^+ inside the sodalite cavities, a signal emerges at 214 ppm, Figure 4c–f. This peak is nearly coincident with the ^{81}Br MAS from bulk AgBr as shown in Figure 4a. The signal at around 214 ppm disappears upon washing the

(15) McMurray, L.; Holmes, A. J.; Kuperman, A.; Ozin, G. A.; Özkar, S. *J. Phys. Chem.* **1991**, *95*, 9448.
(16) Jelinek, R. Ph.D. Thesis, in preparation.
(17) Haase, J.; Pfeifer, H.; Oehme, W.; Klinowski, J. *Chem. Phys. Lett.* **1988**, *150*, 189. Haase, J.; Park, K. D.; Guo, K.; Timken, H. K. C.; Oldfield, E. *J. Phys. Chem.* **1991**, *95*, 6996.

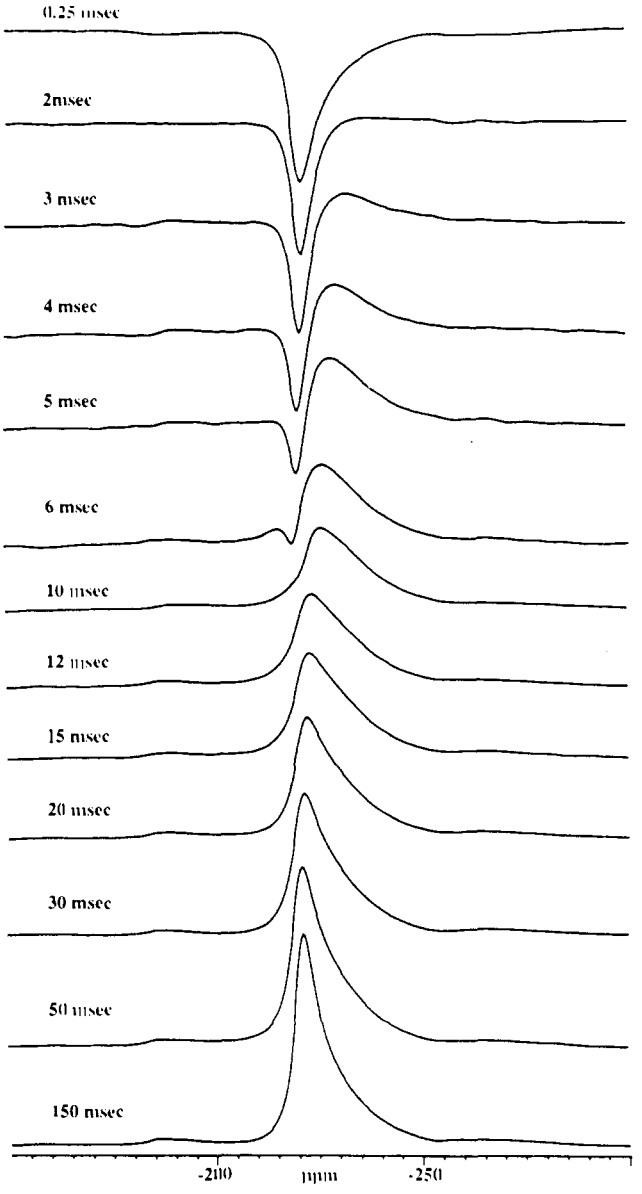

Figure 3. Room-temperature ^{81}Br MAS spectra of sodium,bromo–sodalite containing ≈15% Br^--free cages. The spectra were taken after different delay times, τ, in the inversion–recovery pulse sequence (180°–τ–90°–acquisition).

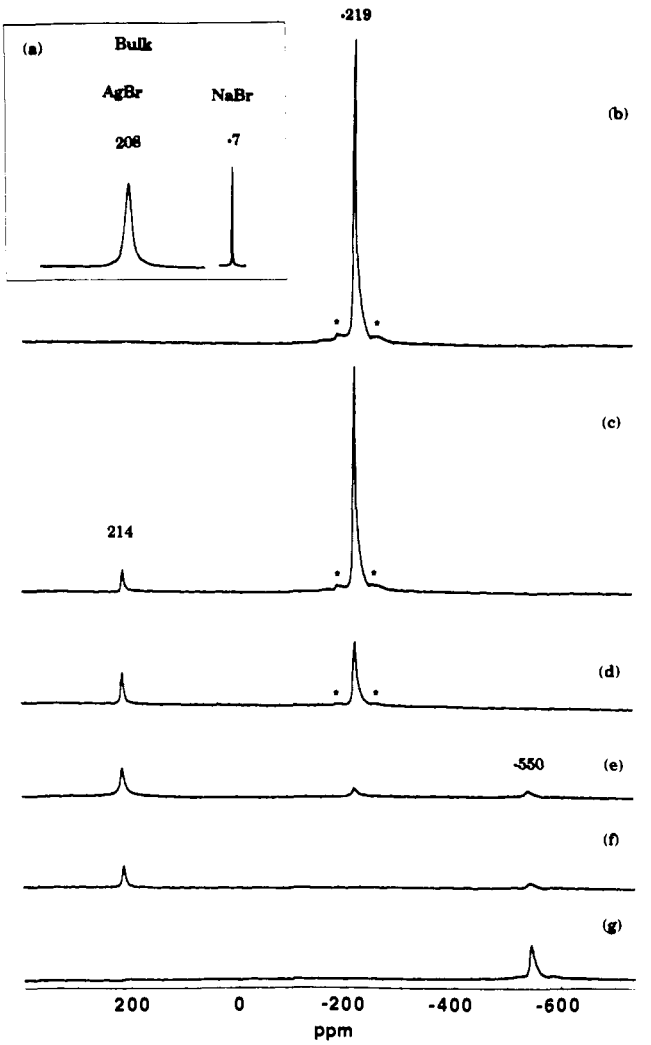

Figure 4. ^{81}Br MAS spectra of (a) bulk NaBr and AgBr, and of Na_8Br_2–sodalite and Ag^+ exchange products: (b) Na_8Br_2–sodalite, (c) $Na_{7.2}Ag_{0.8}Br_2$–sodalite, (d) $Na_6Ag_2Br_2$–sodalite, (e) $Na_4Ag_4Br_2$–sodalite, (f) $Na_{2.8}Ag_{5.2}Br_2$–sodalite, and (g) Ag_8Br_2–sodalite. The asterisks indicate spinning sidebands.

solid sample with aqueous $Na_2S_2O_3$; thus, it is assigned to small quantities of crystalline AgBr, formed through the Ag^+-cation-exchange process. The bulk AgBr phase was not detected by other techniques, like powder X-ray diffraction (PXRD)[6], which indicates that AgBr is essentially formed in nanosize domains, probably on the outer surface of the sodalite crystallites.

The total intensity of the ^{81}Br signal decreases as more Ag^+ cations are loaded within the sodalite framework, as shown in Figure 4. The decrease of the overall signal is due to the formation of mixed-cation clusters, $Na_{4-x}Ag_xBr$. The Ag^+ cations in these clusters form a strong covalent bond with the Br^- anion[4], causing a significant distortion of the charge distribution around the bromide anion. This produces substantial quadrupolar interactions at the Br^- nuclei which broaden and spread the ^{81}Br signal over a large frequency range. A similar broadening effect for quadrupolar ^{23}Na nuclei was recently observed in dehydrated sodalites.[7]

In the final stages of the Ag^+ exchange, Figure 4e–g, a distinct signal appears at around −550 ppm, which becomes the most dominant peak in the spectrum of the fully Ag^+-exchanged sample, Ag_8Br_2–sodalite, as shown in Figure 4g. The upfield signal at −550 ppm is ascribed to encapsulated Ag_4Br clusters. Note the profound upfield shift observed for the Br^- anions, from −219 ppm in the starting Na_4Br clusters to −550 ppm in the completely Ag^+-cation-exchanged sample. The increased shielding of the Br^- nuclei in the encapsulated Ag_4Br clusters looks extraordinary, in particular since a higher covalent nature of the Ag–Br bonds, compared to the respective Na–Br bonds in the Na_4Br clusters, is expected. An increased covalency would reduce the density of electronic charge around the ^{81}Br nuclei, leading accordingly to a *deshielding* effect. This is indeed demonstrated in the ^{81}Br MAS spectra of the bulk NaBr and AgBr, Figure 4a, where deshielding of the ^{81}Br nuclei is observed in the latter material.

The significant shielding of the Br^- anions might be related to changes in the charge distribution inside the sodalite cavities, which occur upon Ag^+ exchange. Previous far-IR spectroscopy[4,5] and ^{23}Na DOR measurements[7] have indicated the emergence of a different charge distribution in the sodalite cavities in silver,-bromo–sodalite. A similar shielding effect was recently observed in ^{77}Se and ^{125}Te NMR studies of CdSe and CdTe clusters encapsulated within sodalite-type frameworks.[18]

To obtain better insight into the environment and nature of the interactions experienced by the Br^- anions during the Ag^+-cation-exchange process, we further examined two related classes of sodium,halo–sodalites. In these experiments, both parent materials, $Na_{6.2}Br_{0.2}[\,]_{1.8}$–sodalite and $Na_{6.4}Br_{0.4}[\,]_{1.6}$–sodalite (where [ ] denotes halide-free cavities), contain high abundances of intentionally synthesized halide-free cavities. The abundant

(18) Moran, K. L.; Ott, A. W.; Gier, T. E.; Harrison, W. T. A.; Eckert, H.; Stucky, G. M. MRS Symposium Series, Boston, Fall 1991.

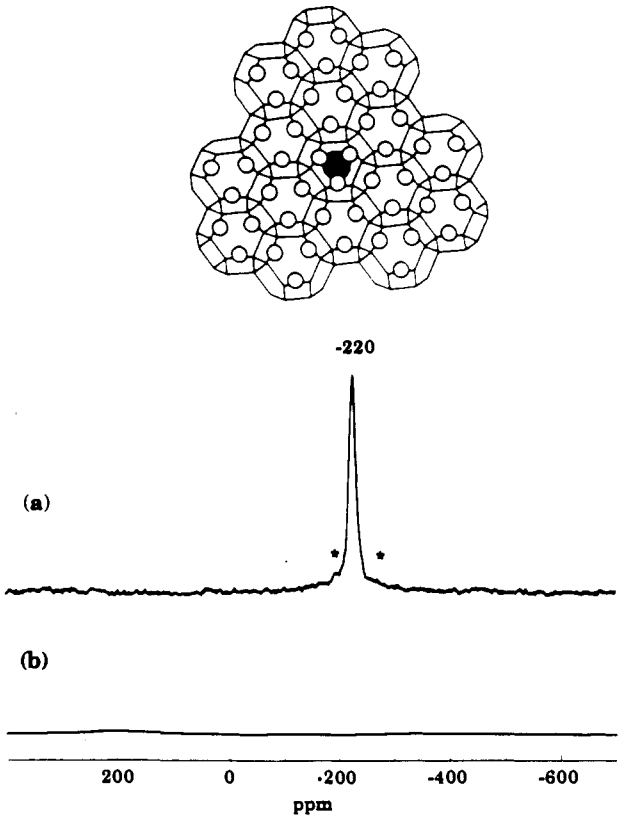

Figure 5. A schematic representation of the sodalite framework showing bromide-containing and bromide-free cavities in an approximately 1:9 ratio, and ^{81}Br MAS spectra of the corresponding materials: (a) $Na_{6.2}Br_{0.2}[\,]_{1.8}$–sodalite and (b) fully Ag^+-exchanged product, $Ag_{6.2}Br_{0.2}[\,]_{1.8}$–sodalite. The black circle represents a Br^- anion inside a cavity and asterisks indicate spinning sidebands.

halide-free cages should prevent interaction between imbibed $Na_{4-x}Ag_xBr$ clusters, thus essentially hosting *isolated* Ag_4Br clusters in the fully Ag^+-exchanged end products.[5,19]

Figure 5 shows the ^{81}Br MAS spectra of $Na_{6.2}Br_{0.2}[\,]_{1.8}$–sodalite and the nominally fully Ag^+-exchanged product. The MAS spectrum of the parent material, $Na_{6.2}Br_{0.2}[\,]_{1.8}$–sodalite, Figure 5a, features a single ^{81}Br resonance at −219 ppm which corresponds to the encapsulated Na_4Br clusters. However, the ^{81}Br MAS spectrum of the fully Ag^+-exchanged material, $Ag_{6.2}Br_{0.2}[\,]_{1.8}$–sodalite, shown in Figure 5b, does not show any signal at −550 ppm. The Ag_4Br clusters in this sample are essentially isolated within a matrix of bromide-empty, water-containing cages. The disappearance of the ^{81}Br signal in Figure 5b is probably due to a distortion of the Ag_4Br tetrahedra within the sodalite cages, probably caused by nearest-neighbor cages. The adjacent water-containing cavities might reduce the symmetry and/or cause distortion of the Ag_4Br clusters, essentially giving rise to a substantial quadrupolar broadening, which would spread the signal over a large spectral area. This observation is consistent with the possibility of a strong interaction between Ag^+ cations in the Br^--containing cages and guests (H_2O molecules and Ag^+ ions) in adjacent cavities within the sodalite framework, as discussed above.

Similar results are obtained for a sample which contains a slightly higher abundance of Br^--containing cavities, as shown in Figure 6. Na_4Br clusters within the parent material, $Na_{6.4}Br_{0.4}[\,]_{1.6}$–sodalite, give rise to the prominent ^{81}Br signal at −219 ppm, Figure 6a. No signal is observed at around −550 ppm in the fully Ag^+-exchanged material, Figure 6a, probably due to the effective isolation of the Ag_4Br clusters within the sodalite lattice. The small ^{81}Br MAS signal observed at around 214 ppm, Figure 6b,c, is again ascribed to traces of bulk AgBr, accumulated on the outer surface of the sodalite crystallites.

(19) Godber, J.; Ozin, G. A. *J. Phys. Chem.* **1988**, *92*, 4980.

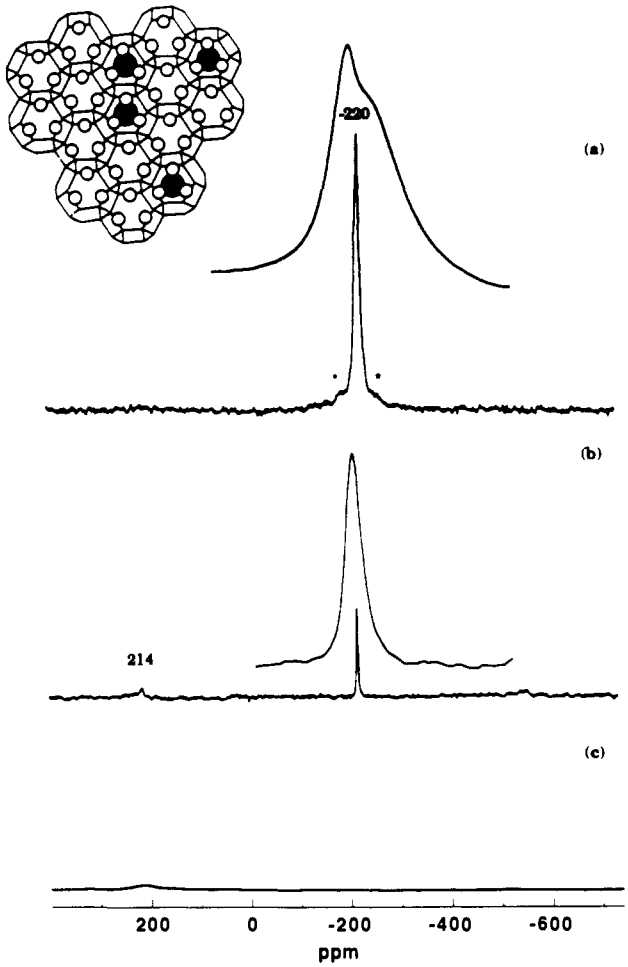

Figure 6. A schematic representation of the sodalite framework showing bromide-containing and bromide-free cavities in an approximately 1:4 ratio, and ^{81}Br MAS spectra of the corresponding materials: (a) $Na_{6.4}Br_{0.4}[\,]_{1.6}$–sodalite, (b) $Na_{0.6}Ag_{5.8}Br_{0.4}[\,]_{1.6}$–sodalite, and (c) fully Ag^+-exchanged product, $Ag_{6.4}Br_{0.4}[\,]_{1.6}$–sodalite. The black circles represent Br^- anions inside a cavity, and the asterisks indicate spinning sidebands.

A particularly interesting result is obtained in the ^{81}Br MAS spectrum of the approximately 90% Ag^+-exchanged sample, $Na_{0.6}Ag_{5.8}Br_{0.4}[\,]_{1.6}$–sodalite, shown in Figure 6b. The ^{81}Br signal at −219 ppm, which is ascribed to the Na_4Br cavities, exhibits a symmetrical Gaussian shape. This observation stands in contrast to the more complex ^{81}Br line shape of the starting material, Figure 6a. The shape of the ^{81}Br signal in Figure 6a is believed to originate from a distribution of Br^--containing- and empty-cage environments within the sodalite lattice; see discussion above. Therefore, the spectrum shown in Figure 6b probably indicates that the Ag^+ cations do not randomly exchange into the sodalite cavities. The NMR spectra apparently indicate that the Ag^+ cations preferentially exchange into Na_4Br cages surrounded by more open, anion-free, Na_3 cavities, rather than the more densely packed anion-containing Na_4Br ones, as observed in Figure 6b. This preferential Ag^+ cation exchange causes the virtual disappearance of the upfield shoulder of the ^{81}Br MAS peak, Figure 6a.

To further check whether there exists a "percolation threshold" between a system of "isolated" and asymmetrical, on one hand, and "interactive" and symmetrical, on the other, Ag_4Br clusters within the sodalite lattice, we examined a sodalite sample which contained a higher ratio of Br^--containing to Br^--empty cavities. Figure 7 shows the ^{81}Br MAS spectra of Ag^+–exchanged $Na_{7.3}Br_{1.3}[\,]_{0.7}$–sodalite. This material hosts a relatively high abundance of Br^- cages, and indeed, as Ag^+ cations are progressively loaded into the sodalite matrix, a peak at −550 ppm emerges and essentially becomes the only ^{81}Br signal in the fully

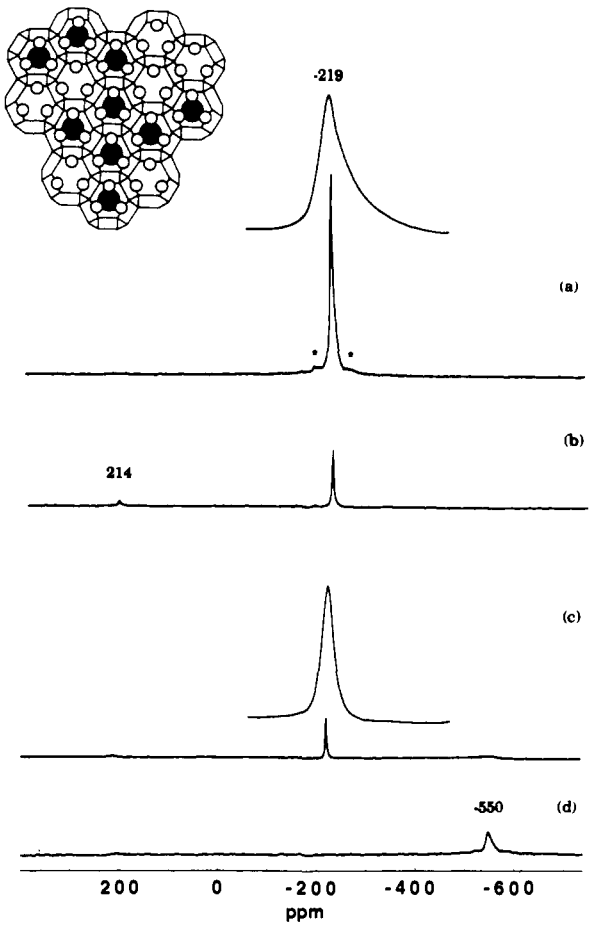

Figure 7. A schematic representation of the sodalite framework showing bromide-containing and bromide-free cavities in an approximately 2:1 ratio, and ^{81}Br MAS spectra of the corresponding materials: (a) $Na_{7.3}Br_{1.3}[\,]_{0.7}$–sodalite, (b) $Na_{5.3}Ag_2Br_{1.3}[\,]_{0.7}$–sodalite, (c) $Na_{0.7}Ag_{6.6}Br_{1.3}[\,]_{0.7}$–sodalite, and (d) fully Ag^+-exchanged product, $Ag_{7.3}Br_{1.3}[\,]_{0.7}$–sodalite. The black circles represent Br^- anions inside a cavity, and the asterisks indicate spinning sidebands.

Ag^+-exchanged sample, Figure 7d. This result stands in contrast to Figures 5 and 6, where the Ag_4Br clusters are essentially isolated among the anion-free cavities, and where no upfield ^{81}Br signal is observed. These results indicate that the interactions of encapsulated Ag_4Br clusters with adjacent Ag_4Br and Br^--empty cages are significantly different.

Note the ^{81}Br MAS spectrum of the 90% Ag^+-exchanged sample, Figure 7c. The Gaussian ^{81}Br line shape of the signal at -219 ppm, ascribed to encapsulated Na_4Br clusters, is different from the asymmetrical peak of the starting material, Figure 7a. This result is similar to the NMR spectrum of $Na_{0.6}Ag_{5.8}Br_{0.4}[\,]_{1.6}$–sodalite, shown in Figure 6b, and again supports the proposal that the Ag^+–exchange process is not statistically random, as discussed above.

^{81}Br Spin–Echo Decay Experiments. To obtain better insight into the properties of the ^{81}Br nuclei in the parent Na_8Br_2–sodalite and the Ag^+-cation-exchanged Ag_8Br_2–sodalite, we estimated the spin–spin relaxation of the ^{81}Br nuclei by performing variable-temperature spin-echo decay experiments. Figure 8 shows the ^{81}Br spin-echo decay measurements of Na_8Br_2–sodalite and Ag_8Br_2–sodalite using a $90°_x$–τ–$180°_x$–acquisition pulse sequence. Similar results were obtained using a solid-echo sequence ($90°_x$–τ–$90°_y$–acquisition). Inspection of Figure 8 reveals that the room-temperature ^{81}Br spin-echo decay, T_2, in the parent sample, Na_8Br_2–sodalite (T_2 = 1.3 ± 0.1 ms; Figure 8a), is significantly longer than the T_2 that was measured for ^{81}Br nuclei in the Ag_8Br_2–sodalite sample (T_2 = 0.6 ± 0.1 ms; Figure 8a). However, the spin-echo decay of the ^{81}Br in Ag_8Br_2–sodalite increases substantially as the temperature is decreased, with T_2 = 1.3 ± 0.1 ms at 85 K, Figure 8b. For Na_8Br_2–sodalite, however,

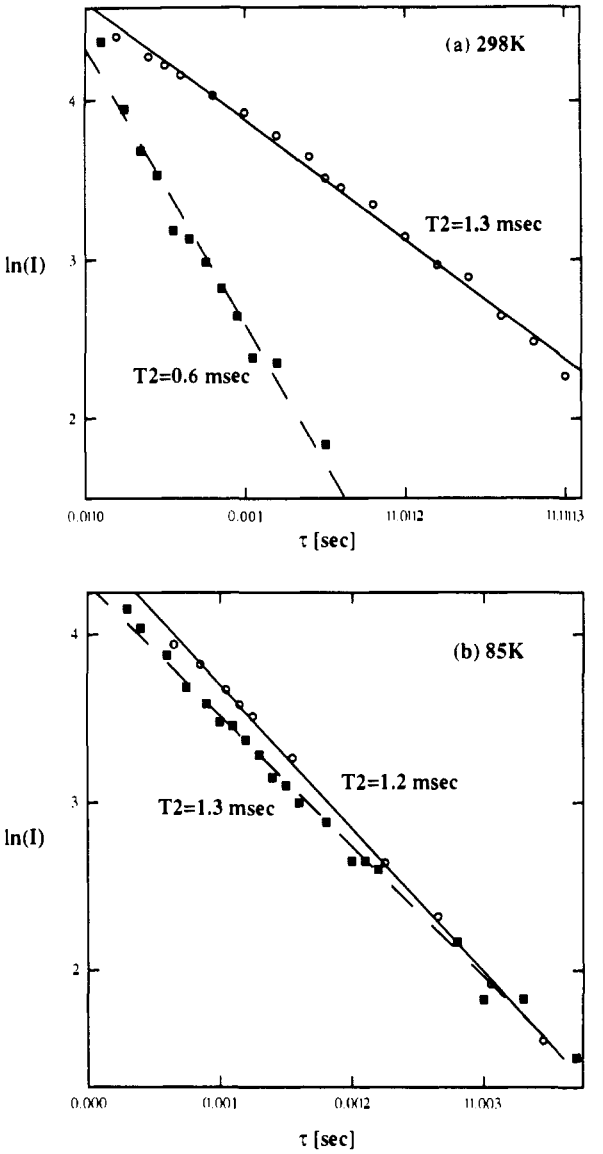

Figure 8. Semilogarithmic plots of static ^{81}Br spin-echo intensities vs delay time, τ, for Na_8Br_2–sodalite (open circles) and Ag_8Br_2–sodalite (filled squares) at (a) room temperature and (b) 85 K. Normalized echo intensities were calculated as the integrated areas of the respective peaks. The T_2 values were calculated from the negative reciprocal slopes. The accuracy of the T_2 values is ±0.1 ms.

no significant change of the ^{81}Br spin-echo decay is observed at lower temperature.

Transverse relaxation of quadrupolar nuclei which exhibit nonzero quadrupolar interaction, such as the ^{81}Br nuclei encapsulated within the sodalite cages, is governed by magnetization dephasing among the central transitions ($^{-1}/_2 \rightarrow {}^{1}/_2$) in the quadrupolar spin system, dipolar interactions to other spins, and motion of the spins.[20] These mechanisms might explain the spin-echo results shown in Figure 8. Second-moment calculations, based on 8 Br^- nearest neighbors at 7.7 Å,[4,6,13] yield a theoretical T_2 of ≈5 ms for ^{81}Br in Na_8Br_2–sodalite and Ag_8Br_2–sodalite. The shorter T_2 actually observed for both samples probably indicates dipolar coupling of the ^{81}Br nuclei to other nuclei in the material, such as ^{27}Al and ^{23}Na (in Na_8Br_2–sodalite), both of which are 100% abundant. The heteronuclear dipolar coupling between the ^{81}Br nuclei and the abundant spins in the material probably results in a spin-echo decay which is determined by the relaxation in the abundant-spin reservoir (spin diffusion).[21] Indeed, second-moment

(20) Abragam, A. *Principles of Nuclear Magnetism*; Oxford University Press: Oxford, 1961.

(21) (a) Han, D. Y.; Kessemeier, H. *Phys. Rev. Lett.* **1991**, *67*, 346. (b) Haase, J.; Oldfield, E. *J. Magn. Reson.*, in press.

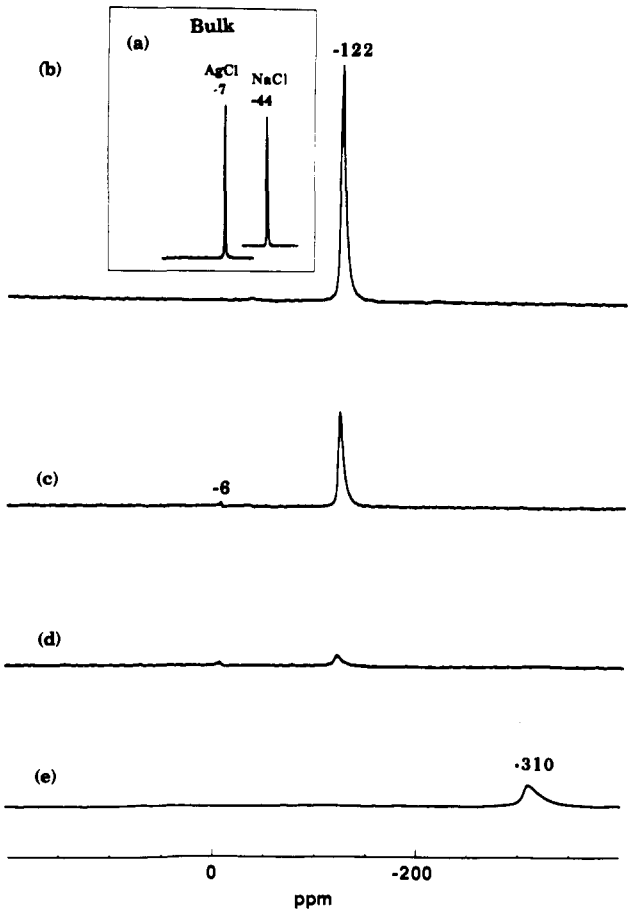

Figure 9. ^{35}Cl MAS spectra of (a) bulk NaCl and AgCl, (b) Na_8Cl_2–sodalite, (c) $Na_7Ag_1Cl_2$–sodalite, (d) $Na_4Ag_4Cl_2$–sodalite, and (e) fully Ag^+-exchanged product, Ag_8Cl_2–sodalite.

calculations yielded significantly bigger second moments, and smaller T_2 values around 1–2 ms, for the ^{23}Na and ^{27}Al nuclei in the sodalite materials studied here.

The faster spin-echo decay of the ^{81}Br nuclei in Ag_8Br_2–sodalite, Figure 8a, is harder to explain within the above framework, since the exchanged Ag^+ cations exhibit a very small gyromagnetic ratio. Thus, their dipolar coupling to the ^{81}Br nuclei and the respective contribution to the spin-echo decay of the ^{81}Br signal would be insignificant. A shorter T_2 for heavy nuclei with s-type character of the electronic inner shell might originate from indirect scalar coupling to unlike spins.[20] However, the change of the spin-echo decay with decreasing temperature, Figure 8, strongly suggests that motion of the Ag^+ cations or the Ag_4Br clusters is affecting the transverse relaxation of the ^{81}Br nuclei.

An experimentally insignificant temperature effect is observed for the T_2 of the ^{81}Br nuclei in Na_8Br_2–sodalite, Figure 8. This probably indicates a more restricted motion of the Na_4Br clusters even at room temperature, and corroborates previous measurements which indicated a higher covalent nature of the Ag–Br bond, compared with the Na–Br bond.[6] This might reduce the electrostatic interaction between the Ag^+ cations and the sodalite framework. Reduced motion of the cations in the sodalite cages at low temperature is also consistent with the contraction of the sodalite unit cell, observed upon decreasing temperature.[22] Further experiments indicate a substantially shorter spin–lattice relaxation rate for ^{81}Br nuclei in Ag_8Br_2–sodalite, compared with Na_8Br_2–sodalite,[16] which again might indicate a less restricted motion in the former material.

^{35}Cl MAS Studies. Encapsulated Na_4Cl tetrahedra are formed within the sodalite cages, in a structurally similar way to that of the sodium,bromo–sodalite system, shown schematically in Figure 1, bottom. ^{35}Cl MAS spectra of Na_8Cl_2–sodalite and its Ag^+-exchanged derivatives are shown in Figure 9. The ^{35}Cl NMR results of the Ag^+-exchange series, Figure 9, are similar to the ^{81}Br spectra of the analogous Br^--containing sodalite materials, Figure 5. A sharp peak at −122 ppm is ascribed to encapsulated Na_4Cl tetrahedra within the sodalite cavities. The position of the signal from the Na_4Cl clusters, at −122 ppm, is further upfield from the bulk NaCl, shown at −44 ppm in Figure 9a, indicating a higher charge density around the encapsulated Cl^- anions.

The intensity of the signal at −122 ppm decreases as Ag^+ cations replace the Na^+, while a small signal appears downfield at −6 ppm. The downfield ^{35}Cl signal is ascribed to a nanocrystalline bulk AgCl phase, formed on the outer surface of the sodalite framework, analogous to the bromo–sodalite system discussed above. The substantially upfield-shifted peak at −310 ppm which appears in the fully Ag^+–exchanged sample, Figure 9e, corresponds to encapsulated Ag_4Cl clusters. The substantial shielding of the ^{35}Cl nuclei might be related to intercavity coupling between adjacent Ag_4Cl clusters, similar to Ag_8Br_2–sodalite, as discussed above.

In order to examine whether the ^{35}Cl MAS resonance from the Na_4Cl clusters exhibits a sensitivity toward adjacent cages, we measured the NMR spectra from samples that contained various amounts of encapsulated Cl^- and I^- anions. Figure 10 shows ^{35}Cl MAS spectra from samples with different Cl^- and I^- compositions, before and after the Ag^+-exchange process. The spectra reveal

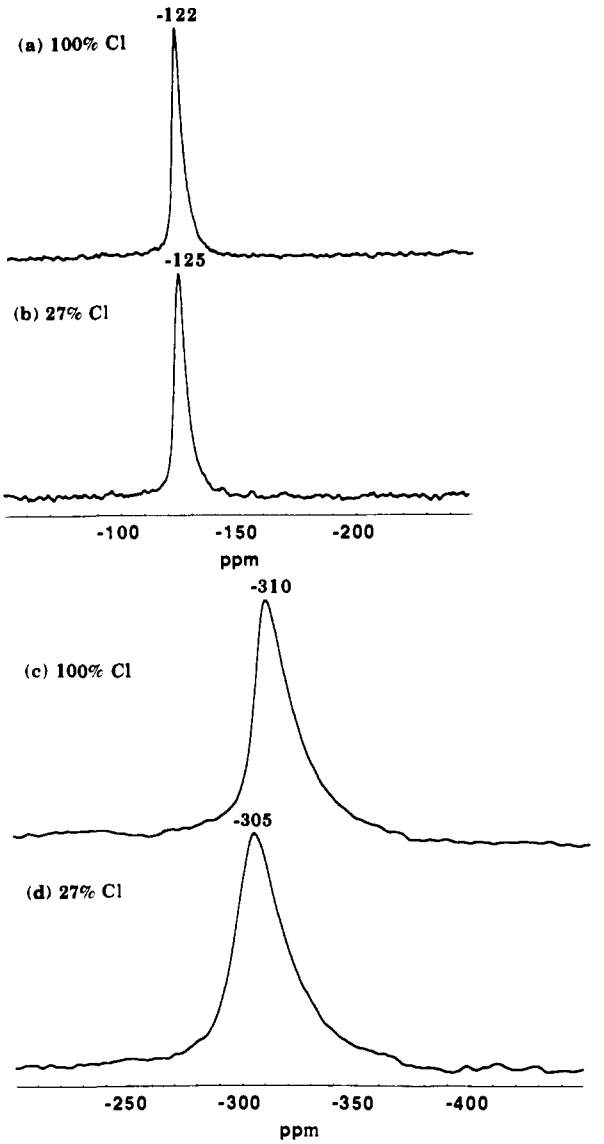

Figure 10. ^{35}Cl MAS spectra of sodalite materials with different Cl^- and I^- compositions, before and after Ag^+ ion exchange: (a) Na_8Cl_2–sodalite, (b) $Na_8Cl_{0.46}I_{1.54}$–sodalite, (c) Ag_8Cl_2–sodalite, and (d) $Ag_8Cl_{0.46}I_{1.54}$–sodalite.

(22) Henderson, C. M. B.; Tailor, D. *Spectrochim. Acta* **1977**, *33a*, 283.

that there is essentially no difference in the shapes of the ^{35}Cl signal between samples that contain no I^- cavities, Figure 10a,c, and sodalite matrices which contain a relatively high abundance of I^- anions, Figure 10b,d. This result is different from the shape sensitivity of the ^{81}Br MAS resonance to anion-empty cavities, Figure 2, which again might indicate that imbibed water molecules in the anion-empty cages have a significant nearest-neighbor effect on the shape of the NMR signal.

However, there is a noticeable change in the *positions* of the ^{35}Cl peaks as I^- anions are distributed in the sodalite lattice. The ^{35}Cl signal, ascribed to encapsulated Na_4Cl tetrahedra, shifts from −122 ppm, Figure 10a, to −125 ppm, Figure 10b, as most of the cavities become occupied with I^- anions. In a similar way, the ^{35}Cl peak, which is ascribed to coupled Ag_4Cl tetrahedra, shifts from −310 ppm, Figure 10c, to −305 ppm, Figure 10d, in the samples that contain 100% and 27% Cl^- anions in the sodalite lattice, respectively. Note that the position of the ^{35}Cl peak from $Ag_8Cl_{0.46}I_{1.54}$–sodalite, Figure 10d, is observed farther *downfield*, relative to the ^{35}Cl peak which arises from Ag_8Cl_2–sodalite, Figure 10c. This relative shift is opposite to the corresponding ^{35}Cl positions, at −125 ppm and −122 ppm, respectively, *before* the Ag^+ exchange, Figure 10b,a.

The unit-cell size of $Na_{8-m}Ag_nCl_{2-m}I_m$–sodalite enlarges with a higher iodide content.[23] Therefore, in the $Na_8Cl_{2-m}I_m$–sodalites, the Na_4Cl clusters experience an enhanced ionicity in the Na_4I-rich sodalite lattice, resulting in a more localized negative charge on the Cl^- anions and the observed upfield shift of 3 ppm, Figure 10a,b. By contrast, the outcome of placing the Ag_4Cl tetrahedra in an increasingly rich Ag_4I lattice could be to slightly change the intracavity interaction between the Ag^+ cation and the Cl^- anion, leading to deshielding of the ^{35}Cl nuclei and the observed downfield shift of 5 ppm, Figure 10c,d.

Conclusions

^{81}Br and ^{35}Cl MAS experiments conducted on silver-exchanged sodium,halo–sodalites yield useful information on the environments of encapsulated clusters within the sodalite lattice. Na_4X (X = Br, Cl) tetrahedra provide a symmetrical environment around the halide anion and give rise to narrow resonances at specific locations in the ^{81}Br and ^{35}Cl MAS spectra. The shape of the ^{81}Br peaks displays a sensitivity toward the distribution of anion-empty cavities within the sodalite matrix, while the positions of the corresponding ^{35}Cl signals exhibit a similar sensitivity to I^--containing cavities. Spin–lattice and spin–spin relaxation measurements provide insight into interactions which involve the ^{81}Br nuclei, as well as motional aspects of the encapsulated clusters.

A strong shielding of the ^{81}Br and ^{35}Cl nuclei is detected, following Ag^+-cation exchange, in sodalite lattices where interaction between adjacent Ag_4Br and Ag_4Cl clusters, respectively, is facilitated. The upfield signal is not detected in samples that contain a high abundance of anion-empty cavities, relative to Br^--containing cavities. A percolation threshold is observed in a sodalite sample with an intermediate ratio of Br^--containing to Br^--empty cavities.

Acknowledgment. This work was supported by the Director, Office of Energy Research, Office of Basic Energy Sciences, Materials and Chemical Sciences Division, U.S. Department of Energy, under Contract No. DEAC03-76SF00098. R.J. is grateful to Professor A. Pines, Dr. J. Haase, and T. Hanna for helpful discussions. G.A.O. wishes to acknowledge the Natural Sciences and Engineering Research Council (NSERC) of Canada's Operating and Strategic Grants Programmes. A.S. would like to thank NSERC for a 1967 Science and Engineering Postgraduate Scholarship.

Poly(arylmethyl) Quartet Triradicals and Quintet Tetraradicals[1]

Andrzej Rajca* and Suchada Utamapanya

Contribution from the Department of Chemistry, University of Nebraska, Lincoln, Nebraska 68588. *Received August 20, 1992*

Abstract: Three poly(arylmethyl) quartet triradicals and three quintet tetraradicals are prepared by oxidation of the corresponding carbanions. The ground states for polyradicals in frozen solutions are established using ESR spectroscopy (4–100 K), including Curie plots (10–80 K), and SQUID magnetometry (2–80 K). For two triradicals and one tetraradical, ESR $\Delta m_s = 2$ transitions are resolved; for one triradical, the $\Delta m_s = 3$ transition is observed. The *i*-Pr-substituted triradical and tetraradical are isolated as solids and studied using SQUID; thermal population of low spin states is negligible at ambient temperature. The most intense bands in the UV–vis spectra for *i*-Pr-substituted tri- and tetraradicals are similar to those found in the homologous diradicals. Electrochemical study of the *i*-Pr-substituted triradical at 195–200 K reveals three reversible voltammetric waves (peaks) that correspond to three one-electron reductions to the corresponding trianion.

Introduction

High-spin organic molecules are closely related to the recent topics of organic magnetism.[2-7] Molecules with many unpaired electrons, which possess high-spin ground states preferred by large margin and stable at ambient temperature, are particularly

(1) This research project was initiated at Kansas State University.

(2) High spin may be defined as parallel alignment of spins for all available unpaired electrons such as $S \geq {}^1/_2$.

(3) For reviews, see: *Proceedings of the Symposium on Ferromagnetic and High Spin Molecular Based Materials*; 197th National Meeting of the American Chemical Society, Dallas, Texas. Miller, J. S.; Dougherty, D. A. *Mol. Cryst. Liq. Cryst.* **1989**, *176*, 1–562. Buchachenko, A. L. *Russ. Chem. Rev.* **1990**, *59*, 307. Iwamura, H. *Adv. Phys. Org. Chem.* **1990**, *26*, 179. Dougherty, D. A. *Acc. Chem. Res.* **1991**, *24*, 88.

(4) High-spin poly(arylmethyl) polyradicals (S = 2–5): (a) Rajca, A.; Utamapanya, S.; Thayumanavan, S. *J. Am. Chem. Soc.* **1992**, *114*, 1884. (b) Rajca, A. *J. Am. Chem. Soc.* **1990**, *112*, 5889. (c) Rajca, A. *J. Am. Chem. Soc.* **1990**, *112*, 5890.

(5) High-spin tetraradicals: (a) Seeger, D. E.; Berson, J. A. *J. Am. Chem. Soc.* **1983**, *105*, 5144, 5146. (b) Seeger, D. W.; Lahti, P. M.; Rossi, A. R.; Berson, J. A. *J. Am. Chem. Soc.* **1986**, *108*, 1251. (c) Berson, J. A. In *The Chemistry of Quinoid Compounds*; Patai, S., Rappaport, Z., Eds.; Wiley: New York, 1988; Vol. II, Chapter 10. (d) Novak, J. A.; Jain, R.; Dougherty, D. A. *J. Am. Chem. Soc.* **1989**, *111*, 7618. (e) Dougherty, D. A. *Mol. Cryst. Liq. Cryst.* **1989**, *176*, 25.

0002-7863/93/1515-2396$04.00/0